Accepted manuscript (author version)

To appear in:

Iranian Journal of Earth Sciences (Iran J. Earth. Sci.)

E-ISSN: 2228-785X Print ISSN: 2008-8779

Received: 20 January 2025

Revised: 22 April 2025

Accepted: 19 June 2025

DOI: https://doi.org/10.57647/j.ijes.2025.17558

Original Research

Experimental study of Di-CaEs solid solution at pressures from 1 atm to 3.0 GPa

Sofja Viktorovna Banushkina[1]*, Zoia Friedrichovna Golitsyna[1], Alexey Anatolyevich Kirdyashkin[1]

[1]*V.S. Sobolev Institute of Geology and Mineralogy, Siberian Branch, Russian Academy of Sciences, Novosibirsk, Russia*

* Corresponding author: banushkinasv@igm.nsc.ru

Abstract

The possibility of 'excess' silica dissolution in clinopyroxene (Cpx) as the calcium molecule of Eskola (CaEs) end member has been known for a long time. Currently, attempts to determine the dependence of non-stoichiometric Cpx compositions on (*P*, *T*)-parameters are ongoing. This article presents data on the analysis of Cpx compositions and the structural and textural features of a phase association obtained from an experimental study of the Di-CaEs cross-section in a 'dry' CMAS system. At atmospheric pressure, the temperature range is 960-1240±10 ºC. At pressures of 1.0-3.0 GPa, the temperature range is 1170-1550±10 ºC. Experiments with synthetic compositions were carried out in a vertical shaft electric resistance furnace with silicon carbide heaters (at atmospheric pressure) and by the quenching method on a piston-cylinder apparatus (at high pressure). It is noted that in the investigated cross-section, two independent stable pyroxene phases are formed: an aluminum-bearing Cpx and a high-magnesian aluminum-free diopside (Di). The composition of clinopyroxene solid solution Cpx(ss) is represented by a quad series of diopside (Di), enstatite (En), calcium molecule of Tschermak (CaTs), calcium molecule of Eskola (CaEs) end members. The diopside phase belongs to the Di-En series. The influence of *P*-*T* parameters and bulk chemical composition on the content of CaEs in Cpx is considered. The trend of eutectic equilibria exists in the temperature range from 1137±10 ºC (at 1 atm) to 1300±10 ºC (at 3.0 GPa). The experimental data obtained can be used in the future to build a physicochemical model of the evolution of quartz-normative rocks.

Keywords: CMAS system; Experimental petrology; Clinopyroxene solid solution; CaEs end member; Geothermobarometry.

1. Introduction

Deviations in the composition of clinopyroxene solid solution Cpx(ss) from stoichiometric values are rare. When studying quartz (Qtz)- and forsterite (Fo)- normative rocks (Yoder and Tilley, 1962; Sobolev et al., 1968) and the calc-alkaline suite of rocks (Ishbulatov, 1977), no quartz was found

in the phase association. It was assumed that 'excess' silica (SiO_2) dissolves in Cpx. This end member has a structural vacancy (Eskola, 1921; Kushiro, 1969; Ishbulatov, 1977), and its crystal-chemical formula is $Ca_{0,5}AlSi_2O_6$ (calcium molecule of Eskola, CaEs). Experiments were carried out in the Di-CaTs-Qtz and Di-Jd-CaTs-Qtz systems (Zharikov et al., 1984; Ishbulatov et al., 1986). Attempts were made to determine the dependence of such non-stoichiometric clinopyroxene compositions on (*P*, *T*)-parameters to use the CaEs end member as an indicator of pressure (Ishbulatov et al., 1986; Gasparik, 2013). The question of whether the CaEs component is a function of pressure, temperature, or bulk chemical composition is still open (Konzett et al., 2008; Zhao et al., 2011; Knapp et al., 2013).

Attempts to derive the polynomial dependence between temperature, pressure and the content of the CaEs component in Cpx were made (Bruno et al., 2002; Ravna and Paquin, 2003; Gonzaga et al., 2010; Talebian Borojenie et al., 2025). An assessment of the influence of alkalis and volatiles was proposed (Schroeder-Frerkes et al., 2016). Mechanisms of Qtz release in eclogites were described (Day and Mulcahy, 2007; Ousta et al., 2024). The problem of seismic heterogeneity at depths of 260-330 km (pressure range of 8.5-11.0 GPa) was considered (Revenaugh and Jordan, 1991; Knapp et al., 2013; Knapp et al., 2015). In particular, it is reported that to achieve the observed wave resistance, ~5-10 mol.% stishovite is required (Williams and Revenaugh, 2005). Authors assumed that it is formed from CaEs-containing Cpx. However, J. Konzett later showed that the CaEs content is insufficient for the formation of the necessary amount of stishovite (Konzett et al., 2008). Similarly, N. Knapp argued that the mechanism suggested with increasing pressure is untenable for the formation of additional SiO_2 in eclogites (Knapp et al., 2015). Consequently, it was concluded that coesite-stishovite transition in eclogites cannot explain the seismic heterogeneity based on the assumption of CaEs existence. As can be seen, the CaEs end member plays an important role in solving geological problems.

To date, experiments have been conducted with both synthetic and natural samples. It is challenging to control the physicochemical conditions of experiments when directly studying natural samples. Therefore, the most informative method is modeling simplified systems of main components, such as the CMAS system. In previous works (Janak et al., 2004; Konzett et al., 2008; Zhao et al., 2011; Schroeder-Frerkes et al., 2016), systems (CMAS+Na) and (CMAS+H_2O) have been investigated. It is important to note that *P-T* ranges vary among different authors in the experiments conducted. Thus, despite the enormous amount of valuable data obtained, there is no strict consistent model. Experiments in a 'dry' CMAS system were conducted to avoid the influence of additional components on the distribution of elements in solid solution (Surkov and Darmenko, 2002). The data obtained demonstrate that there are more complicated phase relationships in the quartz-normative part of the CMAS system.

This article is devoted to a more detailed study of clinopyroxene compositions in the Di-CaEs section of the 'dry' CMAS system. In our work, the compositions of Cpx(ss) previously known (at 2.0-3.0 GPa) are clarified, and new data on compositions at 1 atm and 1.0-1.5 GPa are presented. The conditions for the emergence of melting in the system are also noted. The phase relationships in associations and the texture features in micro-sections are shown. A correlation between the content of CaEs and CaTs end members and the amount of aluminum in Cpx is also demonstrated.

2. Materials and Methods

2.1. Starting materials

The starting materials are oxides (CaO, MgO, Al_2O_3, SiO_2) calcined in platinum (Pt) crucibles. Bulk compositions of stoichiometric Di and CaEs are obtained by the weight method, followed by calcination and grinding. The use of an agate mortar as in works (Knapp et al., 2013), can lead to an increased content of SiO_2 in the run products. Therefore, we use a carbide mortar for grinding the starting silicate compounds. The final grain size is ~5–10 μm. Then, Di and CaEs are mixed. Clear homogeneous glasses are synthesized in a Pt crucible at 1500-1620 ºC for 3-4 hours in a furnace, followed by quenching in distilled cold water. Such glasses imply a homogeneous distribution of material. The method of preparing the starting material is described in detail in our article (Banushkina et al., in press). The ratio of Di and CaEs in the starting material is shown (Fig. 1).

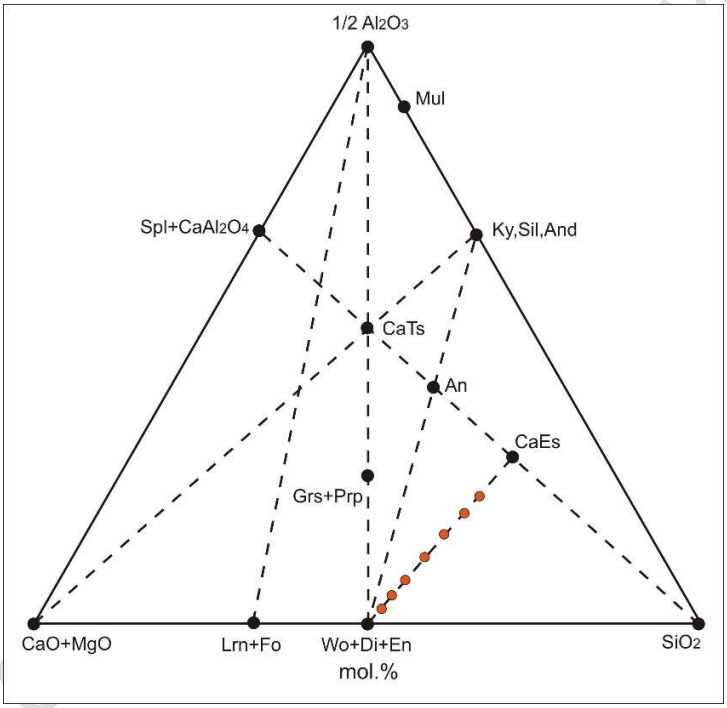

Figure 1. Starting compositions (red points) plotted in the diagram (CaO+MgO) - $1/2Al_2O_3$ - SiO_2. Di - diopside, En - enstatite, Wo - wollastonite, Lrn - larnite, Fo - forsterite, Grs - grossular, Prp - pyrope, CaTs - calcium molecule of Tschermak, CaEs - calcium molecule of Eskola, An - anorthite, Ky - kyanite, Sil - sillimanite, And - andalusite, Spl - spinel, Mul - mullite.

2.2. Experimental equipment and analytical methods

We use piston-cylinder equipment to synthesize the silicate system phases at pressures of 1.0-3.0 GPa and temperatures of 1170-1500±10 °C. The starting composition is loaded into a platinum capsule (wall thickness: 0.5 mm, initial height: 5 mm, final height: about 2–3 mm). It is calcined at 1000 °C during for 6 hours and sealed with an electric welding apparatus. A detailed description of the piston-cylinder apparatus and heating device is provided in our article (Banushkina et al., in

press). The pressure is defined as the load pressure, with a correction amount for friction and losses in the hydraulic system of 0.16 GPa. This was determined by the excess pressure of the Bi(I-II) – Bi(II-III) transition at room temperature and 2.54 GPa. Bismuth wire was placed into a silver chloride tablet directly above the working rod. Calibration at 1200 ºC was carried out using the Qtz-Coes transition. Coesite with quartz seeds turns into quartz at 3.6 GPa; quartz with coesite seeds turns into coesite at 3.7 GPa. In our experiments, the accuracy of pressure measurement is 0.03 GPa, and the accuracy of temperature measurement is 1ºC.

We use a vertical shaft electric resistance furnace with silicon carbide heaters to conduct experiments at atmospheric pressure. The temperature range is 960-1240±10 °C. The device is installed at the V.S. Sobolev Institute of Geology and Mineralogy of the Siberian Branch of the Russian Academy of Sciences (Novosibirsk, Russia). It has not been previously published in periodicals. Temperature variations from the set value did not exceed ±1 °C. The furnace is a vertical cylinder (Fig. 2). Fireclay (7) is used as heat-insulating material. There is an alundum pipe with a diameter of 120 mm inside the furnace body. The upper and lower parts are closed with a heat-insulating cover made of asbestos cement (5, 11). Eight silicon carbide rods acting as heating elements (10) are fixed along the pipe. Current is supplied through electric drives (4). In the middle part of the furnace, an alundum crucible (8) is suspended on a ceramic tube (3). Pt capsules with test samples (9, 14) calcined and sealed by an electric welding apparatus, are placed into the crucible. The capsule size is 6 mm high, 3.5-4.5 mm wide, and the wall thickness is 0.5 mm. The thermocouple junction (1) is adjacent to the Pt capsules. Temperature is monitored by Pt/Pt-Rh10 thermocouples. The cold ends of the thermocouple are led to copper contacts. The temperature is measured with a TA-4 mercury thermometer (accuracy of 0.1 °C). The electromotive force (EMF) of the thermocouple is measured by an F-283 digital DC voltmeter. The samples are quenched by lowering the alundum crucible into distilled water. The entire quenching procedure to room temperature did not exceed 3-5 seconds in duration.

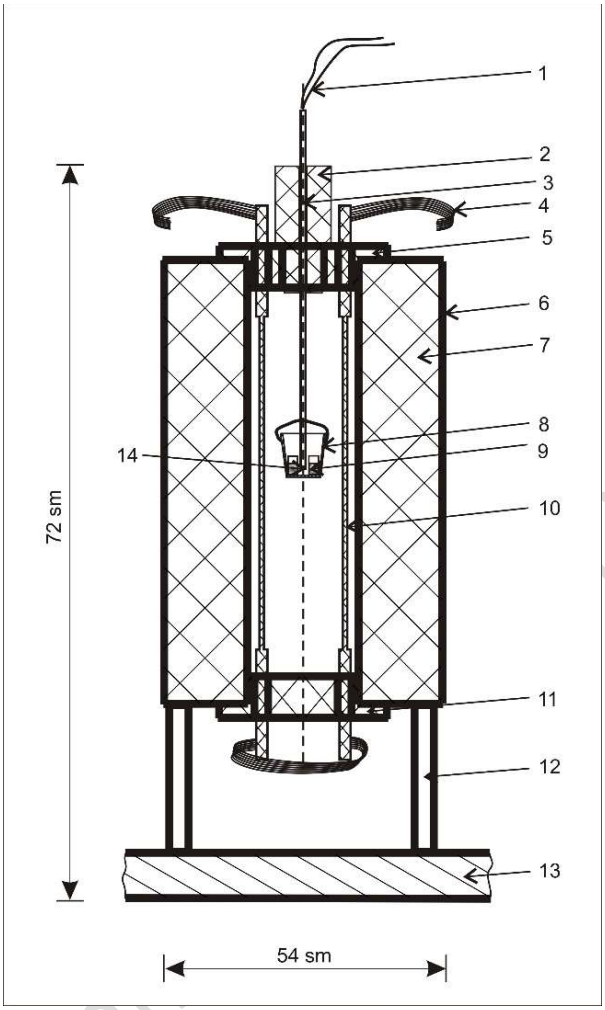

Figure 2. Scheme of electric resistance furnace for conducting experiments at atmospheric pressure. 1 - thermocouple, 2 - heat-insulating plug, 3 - ceramic tube (crucible suspension), 4 - electric drives, 5 - upper heat-insulating cover, 6 - electric furnace body, 7 - thermal insulation, 8 - alundum crucible, 9 – Pt capsules with samples, 10 - silicon carbide heating rods, 11 - lower heat-insulating cover, 12 - supports, 13 - table, 14 - thermocouple junction.

Samples obtained are embedded in epoxy and polished with diamond pastes. The use of diamond pastes avoids a possible increase in silica during sample analysis. Then, double-sided polished sections are made. Phase compositions are determined using a Comebax-Micro electron probe microanalyzer and a MIRA 3 LMU scanning electron microscope (Tescan Orsay Holding) equipped with an INCA Energy 450 XMax80 microanalysis system (Oxford Instruments Nanoanalysis Ltd.). Energy-dispersive X-ray spectra are recorded in the scanning mode. A small raster of 5–50 μm is used for minerals, and 50–500 μm for a quenched melt. The accelerating voltage is 20 kV, the electron beam current is 1.5 nA, and the counting time is 20 s (Lavrent'ev et al., 2015).

It should be noted that in the case of fine-grained samples, EPMA provides a total analysis of several grains of different phases. In practice, this corresponds to the average chemical bulk

composition with small variations in the direction of any prevailing phase. Therefore, we consider energy-dispersive spectrometry for chemical spot analysis of phases preferable due to its high spatial resolution.

Additional phase diagnostics are performed using a RAMAN spectrometer (Horiba Jobin YVON LabRam HR800) with a 532-μm Nd solid-state laser. The spectra are obtained at ambient conditions in backscattering geometry with a laser power of about 1 mW and a spectral resolution of 2 cm^{-1}. The wavenumbers (wavelengths) are calibrated using the emission lines of a Ne lamp (585.25 μm and 540.06 μm). The phase spectrum standards are taken from the Database of Raman Spectroscopy, X-ray Diffraction, and Chemistry of Minerals (http://rruff.info/).

3. Results

3.1. Textures and phase relations

Experiment conditions and results are presented in Table 1.

Table 1. Experimental conditions and results

No. exp.	**A141**	**A140**	**A146**	**A147**	**A148**	**A145**	**A144**	**A143**
x_i [(1)]	0	5	10	15	20	30	50	70
P	1 atm	1 atm	1 atm	1 atm	1 atm	1 atm	1 atm	1 atm
***T*, °C**	1238±10	1238±10	1238±10	1238±10	1238±10	1238±10	1238±10	1238±10
t, hour	53	53	53	53	53	53	53	53
Phases[(2)]	Di	Cpx, An, Tr	Cpx, An, Tr	Cpx, An, Tr	Cpx, An, Tr	L[(3)], Di	L, Di, An	L, An
No. exp.	A142	A104	A103	A102	A101	A100	A99	A98
x_i [(1)]	100	5	10	15	20	30	50	70
P	1 atm	1 atm	1 atm	1 atm	1 atm	1 atm	1 atm	1 atm
***T*, °C**	1238±10	1208±10	1208±10	1208±10	1208±10	1208±10	1208±10	1208±10
t, hour	53	75	75	75	75	75	75	75
Phases[(2)]	An, Tr	Cpx, An, Tr	Cpx, An, Tr	Cpx, An, Tr	Cpx, An, Tr	Di, Cpx, Tr	L, Di, An	L, An
No. exp.	A109	A105	A107	A108	A110	A111	A106	A112
x_i [(1)]	5	10	15	20	30	50	70	5
P	1 atm	1 atm	1 atm	1 atm	1 atm	1 atm	1 atm	1 atm
***T*, °C**	1137±10	1137±10	1137±10	1137±10	1137±10	1137±10	1137±10	1114±10
t, hour	149	149	149	149	149	149	149	173.5
Phases[(2)]	Cpx, An, Tr	Cpx, An, Tr	Cpx, An, Tr	Cpx, An, Tr	Cpx, An, Tr	Cpx, Di, An, Tr	Cpx, Di, An, Tr	Cpx, An, Tr
No. exp.	A114	A116	A118	A113	A117	A115	A119	A120
x_i [(1)]	10	15	20	30	50	70	5	10
P	1 atm	1 atm	1 atm	1 atm	1 atm	1 atm	1 atm	1 atm
***T*, °C**	1114±10	1114±10	1114±10	1114±10	1114±10	1114±10	1067±10	1067±10
t, hour	173.5	173.5	173.5	173.5	173.5	173.5	170.5	170.5
Phases[(2)]	Cpx, An, Tr	Cpx, An, Tr	Cpx, An, Tr	Cpx, An, Tr	Cpx, Di, An, Tr	Cpx, Di, An, Tr	Cpx, An, Tr	Cpx, An, Tr

No. exp.	A121	A122	A123	A124	A125	A126	A127	A128
x_i (1)	15	20	30	50	70	5	10	15
P	1 atm	1 atm	1 atm	1 atm	1 atm	1 atm	1 atm	1 atm
***T*, ºC**	1067±10	1067±10	1067±10	1067±10	1067±10	1013±10	1013±10	1013±10
t, hour	170.5	170.5	170.5	170.5	170.5	198.5	198.5	198.5
Phases(2)	Cpx, An, Tr	Cpx, An, Tr	Cpx, An, Tr	Cpx, Di, An, Tr	Cpx, Di, An, Tr	Cpx, An, Tr	Cpx, An, Tr	Cpx, An, Tr
No. exp.	A129	A130	A132	A133	A136	A134	A135	P-487
x_i (1)	20	30	50	70	10	15	20	30
P	1 atm	1 atm	1 atm	1 atm	1 atm	1 atm	1 atm	1.0 GPa
***T*, ºC**	1013±10	1013±10	1013±10	966±10	966±10	966±10	966±10	1363±10
t, hour	198.5	198.5	198.5	414	414	414	414	4
Phases(2)	Cpx, An, Tr	Cpx, An, Tr	Cpx, Di, An, Tr	Cpx, An, Tr	Cpx, An, Tr	Cpx, An, Tr	Cpx, An, Tr	Di, L
No. exp.	P-489	P-488	P-565	P-564	P-555	P-481	P-562	P-561
x_i (1)	50	70	30	50	30	30	30	50
P	1.0 GPa	1.0 GPa	1.0 GPa	1.0 GPa	1.0 GPa	1.0 GPa	1.0 GPa	1.0 GPa
***T*, ºC**	1363±10	1363±10	1335±10	1335±10	1301±10	1300±10	1293±10	1293±10
t, hour	4	4	7	7	8.5	6	7.5	7.5
Phases(2)	Di, L	An, Di, L	Cpx, Di, L	Di, L	Cpx, Di, L	Cpx, Di, L	Cpx, Di, L	An, Di, L
No. exp.	P-567	P-568	P-569	P-558	P-554	P-551	P-478	P-509
x_i (1)	50	60	70	30	30	30	30	10
P	1.0 GPa	1.0 GPa	1.0 GPa	1.0 GPa	1.0 GPa	1.0 GPa	1.0 GPa	1.0 GPa
***T*, ºC**	1281±10	1281±10	1281±10	1275±10	1261±10	1230±10	1227±10	1208±10
t, hour	7	7	7	12	7.5	25	25	17.5
Phases(2)	An, Di, L	An, Di, L	An, Di, L	Cpx, Di, L	Cpx, Di, L	Cpx, Di, L	Cpx, Di, L	Cpx, Di, L
No. exp.	P-510	P-511	P-523	P-522	P-521	P-526	P-525	P-524
x_i (1)	20	30	10	20	30	10	20	30
P	1.0 GPa	1.0 GPa	1.2 GPa	1.2 GPa	1.2 GPa	1.3 GPa	1.3 GPa	1.3 GPa
***T*, ºC**	1208±10	1208±10	1208±10	1208±10	1208±10	1208±10	1208±10	1208±10
t, hour	17.5	17.5	19	19	19	16	16	16
Phases(2)	Cpx, Di, L	Cpx, Di, L	Cpx, An	Cpx, An	Qtz, An, Cpx, Di	Cpx, An	Cpx, An	Qtz, An, Cpx, Di
No. exp.	P-536	P-535	P-534	P-497	P-498	P-499	P-503	P-504
x_i (1)	10	20	30	10	20	30	10	20
P	1.4 GPa	1.4 GPa	1.4 GPa	1.5 GPa	1.5 GPa	1.5 GPa	1.5 GPa	1.5 GPa
***T*, ºC**	1208±10	1208±10	1208±10	1222±10	1222±10	1222±10	1171±10	1171±10
t, hour	12	12	12	12	12	12	20	20
Phases(2)	Cpx, An	Cpx, An	Qtz, An, Cpx, Di	Cpx	An, Cpx	An, Cpx	Qtz, An, Cpx	Qtz, An, Cpx
No. exp.	P-505	P-474	P-476	P-475	P-462	P-463	P-464	P-471
x_i (1)	30	20	30	50	20	30	40	20
P	1.5 GPa	2.0 GPa	2.0 GPa	2.0 GPa	2.0 GPa	2.0 GPa	2.0 GPa	2.0 GPa
***T*, ºC**	1171±10	1470±10	1470±10	1470±10	1417±10	1417±10	1417±10	1367±10
t, hour	20	5.5	5.5	5.5	6.5	6.5	6.5	9.5

Phases[2]	Qtz, An, Cpx, Di	Cpx, Di, L	Cpx, L	Cpx, L	Cpx, Di, L	Cpx, Di, L	Cpx, Di, L	Cpx, Di, L
No. exp.	P-472	P-473	P-465	P-467	P-466	P-469	P-468	P-470
x_i [1]	30	50	20	30	50	20	30	50
P	2.0 GPa	2.0 GPa	2.0 GPa	2.0 GPa	2.0 GPa	2.0 GPa	2.0 GPa	2.0 GPa
***T*, °C**	1367±10	1367±10	1300±10	1300±10	1300±10	1218±10	1218±10	1218±10
t, hour	9,5	9,5	16,5	16,5	16,5	38	38	38
Phases[2]	Cpx, Di, L	Cpx, Di, L	Cpx, Di, L	Cpx, Di, L	Cpx, Di, L	Cpx, Di, An, Qtz	Cpx, Di, An, Qtz	Cpx, Di, An, Qtz
No. exp.	P-451	P-450	P-42	P-448	P-447	P-454	P-45	P-457
x_i [1]	30	50	20	30	50	10	20	10
P	3.0 GPa	3.0 GPa	3.0 GPa	3.0 GPa	3.0 GPa	3.0 GPa	3.0 GPa	3.0 GPa
***T*, °C**	1547±10	1547±10	1525±10	1522±10	1522±10	1518±10	1475±10	1441±10
t, hour	3.5	3.5	3	3	3	0.3	5	5
Phases[2]	Cpx, Di, L	Cpx, L	Cpx, Di, L	Cpx, Di, L	Cpx, L	Cpx, Di, L	Cpx, Di, Grt, L	Cpx, Di, Qtz, L
No. exp.	P-458	P-48	P-459	P-461	P-439	P-438	P-56	P-442
x_i [1]	50	20	10	70	30	50	20	30
P	3.0 GPa	3.0 GPa	3.0 GPa	3.0 GPa	3.0 GPa	3.0 GPa	3.0 GPa	3.0 GPa
***T*, °C**	1441±10	1425±10	1422±10	1422±10	1420±10	1420±10	1371±10	1317±10
t, hour	5	6	7	7	8	8	6	18
Phases[2]	Cpx, Grt, L	Cpx, Di, Grt, L	Cpx, Di, Qtz	Cpx, L	Cpx, Di, Grt, L	Cpx, Grt, L	Cpx, Di, Grt, L	Cpx, Di, Grt, L
No. exp.	P-441	P-445	P-444					
x_i [1]	50	30	50					
P	3.0 GPa	3.0 GPa	3.0 GPa					
***T*, °C**	1317±10	1219±10	1219±10					
t, hour	18	38	38					
Phases[2]	Cpx, Grt, Qtz	Cpx, Di, Grt, Qtz	Cpx, Grt, Qtz, Ky					

Note. [1] x_i - CaEs, mol.%; [2] phases diagnosed in the run products; [3] L - glass

Experiments at 1 atm were carried out in the temperature range of 960-1240 °C. Crystalline phases are represented by an assemblage Cpx(ss) + Di + An + Tr. Large grains of Cpx, with a size of approximately 200-600 μm (Fig. 3a), are formed with a small amount of CaEs in the bulk composition. As the CaEs component increases, feathery (Fig. 3b) and fibrous (Fig. 3c) grains are formed, and granularity decreases (Fig. 3d). Fine-grained microstructures (crystal sizes of ~1-10 μm) and close intergrowth of coexisting phases are noted at low temperatures. The microstructures formed depend on (*P*, *T*)-parameters and the bulk composition of the system. Subsequent EDS showed phase identity and homogeneity of composition over the entire area of the section. There is no zoning or variation in grain composition, suggesting the achievement of equilibrium.

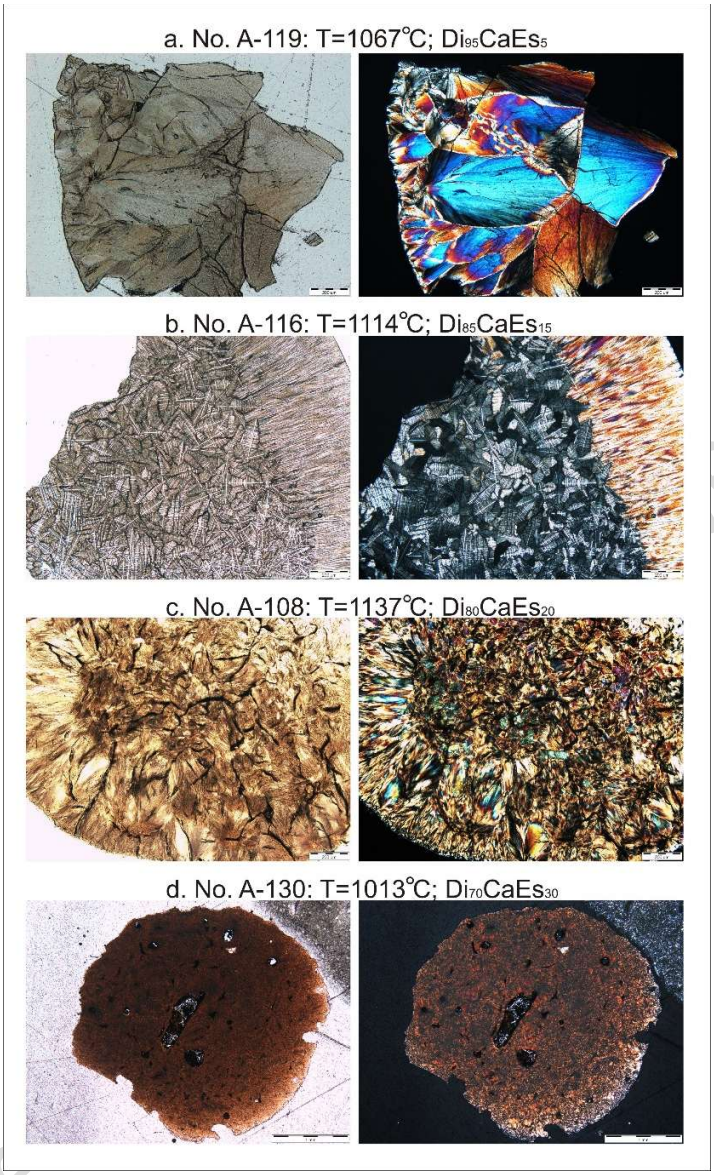

Figure 3. Microstructures of aluminum-bearing clinopyroxenes Cpx(ss) in the run products in the solidus field at 1 atm in plane polarized light (left) and crossed polarizers (right). (a) large grains of Cpx; (b) feathery microstructure is characterized by a pronounced kernel in the grains; (c) fibrous microstructure; (d) fine-grained microstructure is represented by close intergrowth of Cpx, An, Tr phases.

Residual microstructures obtained characterize a change in crystallization conditions in the solidus field. To confirm this, we annealed the stoichiometric diopside glass at 1100 °C (Fig. 4) and observed a similar microstructure. This indicates that the microstructures from our experiments are formed under solidus conditions, rather than by quenching the melt.

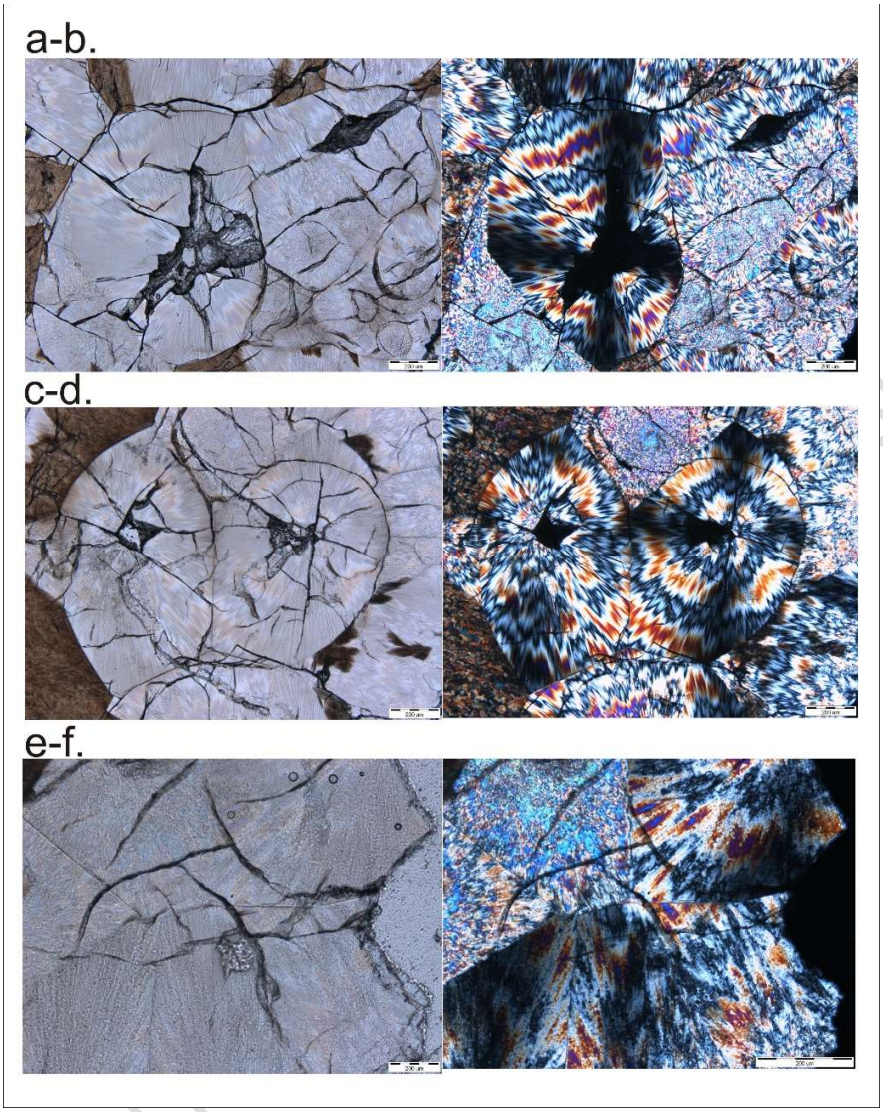

Figure 4. Microstructures of annealed stoichiometric diopside glass at 1100 °C, 1 atm in plane polarized light (a, c, e) and crossed polarizers (b, d, f). Experiment duration: 1 h (a-b); 24 h (c-d); 72 h (e-f).

In the solidus field, An and Tr grains are too small for visual identification. However, Raman spectra of the samples indicate that An and Tr are located directly in the Cpx matrix (Fig. 5).

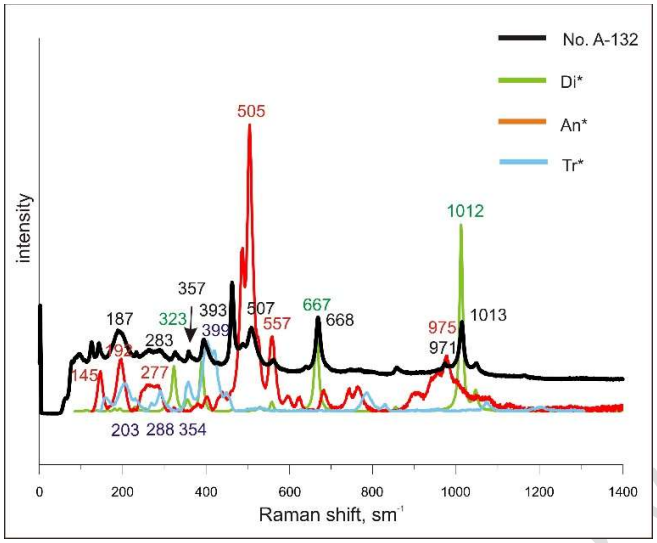

Figure 5. Raman spectra of sample No.A-132 (CaEs content 50 mol.%, 1 atm, 1013±10 °C). The phases obtained are Cpx, Di, An, Tr. The phase spectrum standards (marked with *) are taken from the Database of Raman Spectroscopy, X-ray Diffraction, and Chemistry of Minerals (http://rruff.info).

We assume that Di has not been previously diagnosed due to the proximity of its optical properties to aluminous Cpx. Its existence is also confirmed by EDS.

Glass (L) was found in experiments at temperatures above 1137 ± 10 °C with a starting CaEs content above 30 mol.%. In the liquidus field, the aluminum-free Di phase is represented both by accumulations of intergrown fine-grained aggregates with a grain size of 1-10 μm (Fig. 6a) and well-faceted crystals up to 250 μm in size, floating in glass (Fig. 6b).

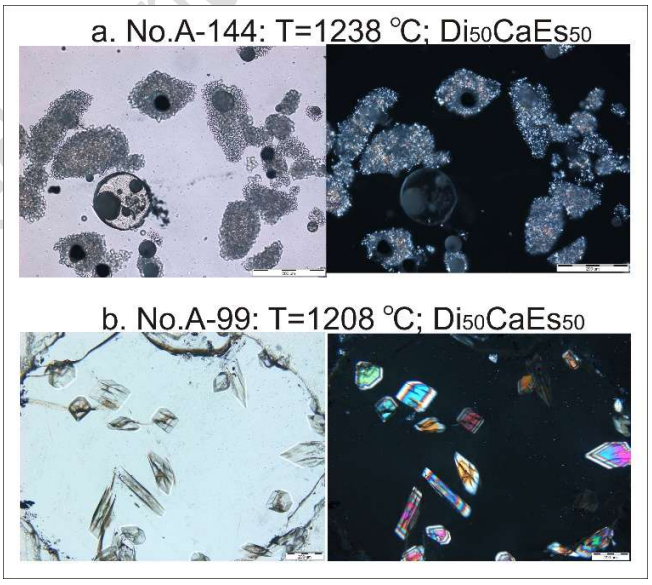

Figure 6. Fine-grained aggregates (a) and well-faceted crystals (b) of aluminum-free diopside Di in the run products in glass at 1 atm in plane polarized light (left) and crossed polarizers (right).

All high-pressure experiments were conducted in the *P-T* range of 1.0-3.0 GPa and 1170-1550 °C. Data on experimental conditions at 2.0-3.0 GPa are taken from works (Surkov et al.,2004; Surkov et al., 2007). Crystalline phases are represented by an assemblage of Cpx(ss) + Di + An + Qtz at pressures up to 2.0 GPa. Garnet (Grt) appears at 3.0 GPa and above 1200 °C. Cpx(ss) form various microstructures, which are explained by the change in crystallization conditions (Fig. 7a-f). EDS shows the identity of Cpx composition over the entire area of the section.

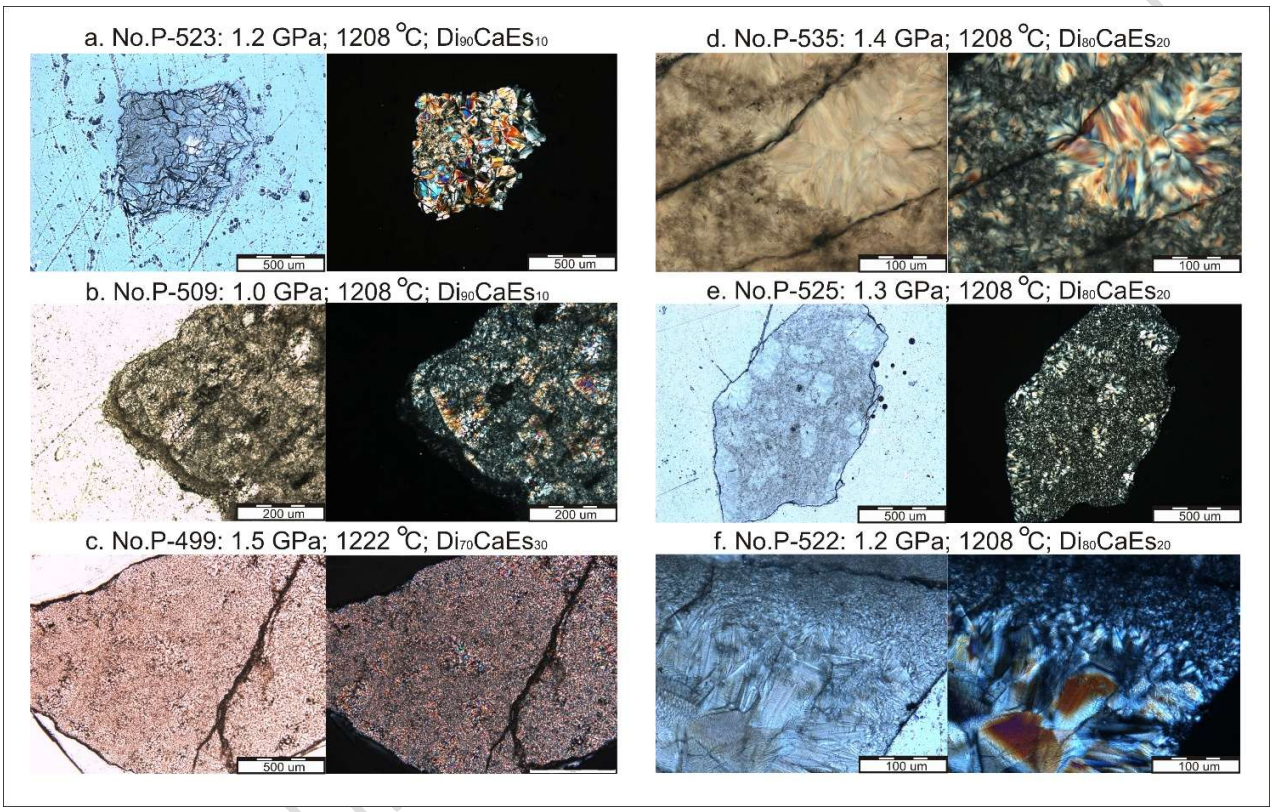

Figure 7. Microstructures of aluminum-bearing clinopyroxenes Cpx(ss) in the run products in the solidus field at high pressure in plane polarized light (left) and crossed polarizers (right). (a-b) large crystalline intergrowth of Cpx grains in the diopside part of the studied cross-section; c) fine-grained aggregates; d) tangled fibrous microstructure; e) grains up to 40 μm in size stand out from a common mass; f) feathery microstructure with a pronounced kernel in the grains.

The presence of aluminum-free Di is reliably diagnosed by EDS. Di also forms close intergrowths with others phases (Fig. 8). Qtz is presented as close intergrowths with An and Cpx (Fig. 8a) and large single crystals with a size of up to ~30-50 μm (Fig. 8b-c). Glass (L) (Fig. 8d) was found in experiments at temperatures above 1208±10 °C (at 1.0 GPa) with a starting CaEs content over 5 mol.%.; above 1250±10 °C (at 2.0 GPa); and above 1300±10 °C (at 3.0 GPa).

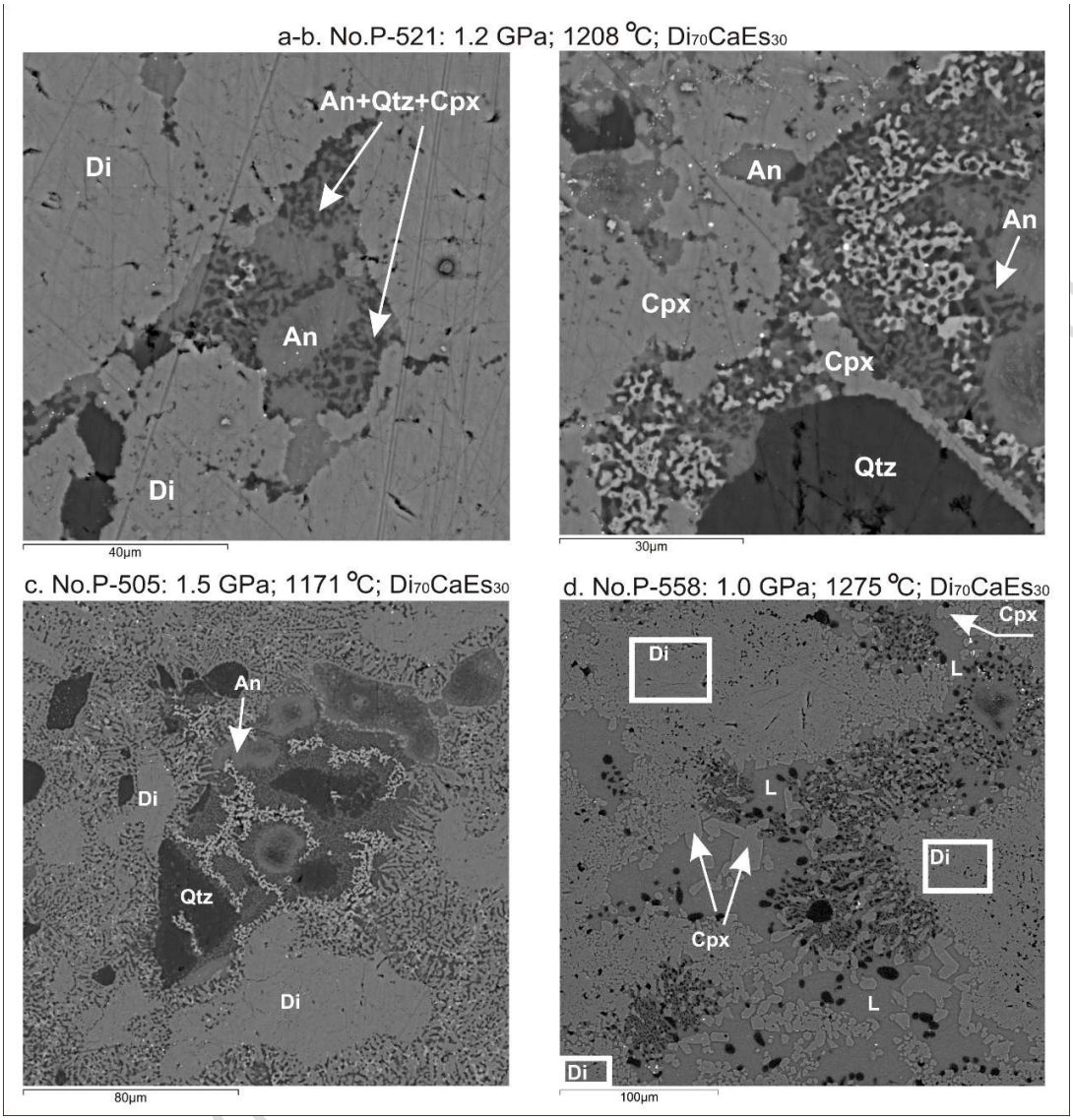

Figure 8. Backscattered electron micrographs of the run products. (a) close intergrowth of Qtz, An, Cpx in the solidus field; (b) large Qtz single crystals in the solidus field; (c) phases Di, Qtz, An, Cpx in the solidus field; (d) glass L appears in experiments at temperatures above 1208±10 ºC.

3.2. Clinopyroxene composition

According to the data obtained, the phase Di composition is characterized by the prevalence of the magnesia component over the calcium one and the absence of aluminum. The amount of enstatite (En) component is up to 5 mol.% (Table 2).

Table 2. Phase diopside compositions in the run products

No. exp.		**A-145**	**A-144**	**A-100**	**A-99**	**A-113**	**P-487**	**P-488**	**P-565**
Analyses(1) wt%	SiO_2	55.71	56.2	54.79	54.79	54.83	55.47	56.16	55.62
	Al_2O_3	0.51	0.64	1.21	1.8	1.87	0	0	1.1
	MgO	18.95	19.47	18.98	18.99	17.71	19.09	19.02	18.84
	CaO	24.84	24.58	24.6	24.35	25.34	25.45	25.42	24.96
	Total	100.01	100.89	99.58	99.93	99.75	100.01	100.6	100.52
a.p.f.u.(2)	Si	1.999	1.997	1.976	1.967	1.976	1.997	2.007	1.986
	Al	0.022	0.027	0.051	0.076	0.079	0.000	0.000	0.046
	Mg	1.014	1.031	1.020	1.016	0.951	1.025	1.013	1.003
	Ca	0.955	0.936	0.951	0.936	0.978	0.982	0.973	0.955
	Total	3.990	3.990	3.998	3.995	3.985	4.003	3.993	3.991
Xmol(3)	Di	94.8	93.6	92.4	90.2	93.9	98.3	98.2	94.1
	En	3.2	5.1	4.4	5.5	0.6	2	1.9	3.3
No. exp.		P-564	P-555	P-562	P-561	P-558	P-567	P-569	P-478
Analyses(1) wt%	SiO_2	56.01	56.16	55.75	57.08	56.16	55.79	56.22	55.69
	Al_2O_3	0.45	0	1.87	0.23	0	0	0.4	0
	MgO	19.34	18.87	18.95	18.79	18.87	18.56	18.01	19.45
	CaO	24.86	25.51	24.47	25.3	25.51	25.45	24.57	25.16
	Total	100.66	100.54	101.04	101.4	100.54	99.8	99.2	100.3
a.p.f.u.(2)	Si	1.997	2.008	1.976	2.018	2.008	2.010	2.028	1.997
	Al	0.019	0.000	0.078	0.010	0.000	0.000	0.017	0.000
	Mg	1.028	1.006	1.001	0.990	1.006	0.997	0.969	1.040
	Ca	0.950	0.977	0.929	0.959	0.977	0.983	0.950	0.967
	Total	3.994	3.992	3.985	3.977	3.992	3.990	3.963	4.003
Xmol(3)	Di	95	98.5	90.5	97.2	98.5	98.3	94	97.2
	En	4.1	1.3	5.2	1.7	1.3	0.7	1.3	3.4
No. exp.		P-521	P-524	P-534	P-505	P-474	P-462	P-471	P-472
Analyses(1) wt%	SiO_2	57.04	55.64	56.18	56.82	55.09	55.84	54.83	54.83
	Al_2O_3	0	0.17	0	0.62	0	0	0	0
	MgO	18.79	18.52	18.14	18.47	18.97	19.97	18.95	18.97
	CaO	25.8	25	25.17	25.33	24.67	24.36	25.31	25.21
	Total	101.63	99.33	99.49	101.24	98.73	100.17	99.09	99.01
a.p.f.u.(2)	Si	2.016	2.011	2.026	2.012	2.005	2.000	1.993	1.994
	Al	0.000	0.007	0.000	0.026	0.000	0.000	0.000	0.000
	Mg	0.990	0.998	0.975	0.975	1.029	1.066	1.027	1.029

	Ca	0.977	0.968	0.973	0.961	0.962	0.935	0.986	0.983
	Total	3.984	3.985	3.974	3.975	3.995	4.000	4.007	4.006
Xmol[3]	Di	99.6	96.2	97.2	96.5	95.3	94.1	97.7	97.4
	En	0.6	1.5	0.1	1.3	3.1	6.1	1.9	2.1
No. exp.		P-473	P-465	P-466	P-469	P-468	P-470	P-42	P-454
Analyses[1] wt%	SiO_2	55.9	55.82	55.64	54.94	55	54.79	55.36	55.88
	Al_2O_3	0.01	0	0	0	0	0	0	0
	MgO	19.24	18.81	19.44	19.12	18.9	18.79	18.81	19.47
	CaO	25.21	25.72	24.98	24.85	25.03	25.26	25.65	24.96
	Total	100.36	100.35	100.06	98.91	98.93	98.84	99.82	100.31
a.p.f.u.[2]	Si	2.002	2.003	1.999	1.998	2.000	1.997	1.998	2.001
	Al	0.000	0.000	0.000	0.000	0.000	0.000	0.000	0.000
	Mg	1.027	1.006	1.041	1.036	1.025	1.021	1.012	1.040
	Ca	0.968	0.989	0.961	0.968	0.975	0.986	0.992	0.958
	Total	3.998	3.997	4.001	4.002	4.000	4.003	4.002	3.999
Xmol[3]	Di	97.3	99.3	96.5	96	96.7	97.5	99.1	96.4
	En	2.8	0.8	3.7	3.1	2.3	1.6	0.9	3.8
No. exp.		P-45	P-457	P-48	P-459	P-439	P-56	P-445	
Analyses[1] wt%	SiO_2	54.72	55.65	56.18	55.45	55.48	55.47	56.43	
	Al_2O_3	0.05	0.05	0.01	0	0.22	0.01	0.01	
	MgO	18.71	19.61	18.86	19.3	18.37	19.48	19.28	
	CaO	25.44	24.9	25.71	25.1	24.85	24.99	24.91	
	Total	98.92	100.21	100.76	99.85	98.92	99.95	100.63	
a.p.f.u.[2]	Si	1.994	1.996	2.006	1.997	2.013	1.996	2.012	
	Al	0.002	0.002	0.000	0.000	0.009	0.000	0.000	
	Mg	1.016	1.048	1.004	1.036	0.994	1.045	1.025	
	Ca	0.993	0.957	0.984	0.969	0.966	0.963	0.951	
	Total	4.005	4.003	3.994	4.003	3.982	4.004	3.988	
Xmol[3]	Di	98.1	96.1	99.3	96.9	95.5	96.5	96.2	
	En	1.1	4.3	1	3.1	1.5	3.8	3.4	

Note. [1] analyses obtained by Energy-dispersive spectrometry (EDS), wt.%; [2] atomic per formula unit on the basis of 6 oxygens; [3] end members, mol.%.

We reanalyzed the data from works (Surkov et al., 2004; Surkov et al., 2007) using energy-dispersive spectrometry. The results obtained are somewhat different from those published earlier. Table 3 shows both new data and data previously published (Surkov et al., 2004; Surkov et al., 2007; Surkov et al., 2018; Banushkina et al., 2019), taking into account the repeated analyses. The

composition of Cpx(ss) is identical in different areas of the sample. It can be expressed by a combination of four end members – Di, En (or Wo), CaTs, and CaEs. As can be seen, compositions do not go beyond the boundaries of these end members (Fig. 9).

Table 3. Compositions of clinopyroxenes in the run products

No. exp.		**A101**	**A102**	**A103**	**A104**	**A105**	**A107**	**A108**	**A109**
Analyses(1) wt%	SiO_2	50.27	50.47	52.25	54.98	52	50.57	51.16	54.6
	Al_2O_3	11.9	10.24	6.42	1.87	9.08	12.22	10.85	3.49
	MgO	16.2	16.57	17.87	19.39	15.93	15.46	15.53	17.39
	CaO	20.61	22.47	22.98	23.62	22.51	21.36	22.02	23.84
	Total	98.98	99.74	99.52	99.86	99.53	99.62	99.56	99.81
a.p.f.u.(2)	Si	1.797	1.804	1.876	1.97	1.858	1.799	1.825	1.964
	Al	0.501	0.431	0.272	0.079	0.382	0.512	0.456	0.148
	Mg	0.863	0.883	0.956	1.035	0.849	0.82	0.826	0.932
	Ca	0.79	0.861	0.884	0.907	0.862	0.814	0.841	0.919
	Total	3.952	3.98	3.988	3.991	3.951	3.945	3.947	3.963
Xmol(3)	Di	53.88	64.51	74.82	86.73	67.07	55.79	61.35	84.49
	En	16.23	11.9	10.41	8.41	8.9	13.09	10.6	4.38
	CaTs	20.26	19.55	12.4	3.02	14.2	20.13	17.55	3.65
	CaEs	9.62	4.04	2.37	1.84	9.83	10.99	10.5	7.49
No. exp.		A110	A111	A112	A114	A115	A116	A117	A118
Analyses(1) wt%	SiO_2	55.44	54.25	54.03	51.9	55.24	49.69	54.2	50.21
	Al_2O_3	5.66	7.39	3.81	8.2	7.27	11.89	11.17	11.71
	MgO	15.36	15.95	17.96	16.52	14.87	15.88	12.1	14.91
	CaO	23.43	23.66	24.02	22.81	22.32	22.02	22.08	22.01
	Total	99.89	101.25	99.82	99.43	99.69	99.48	99.54	98.83
a.p.f.u.(2)	Si	1.97	1.907	1.938	1.861	1.957	1.778	1.915	1.805
	Al	0.237	0.306	0.161	0.346	0.303	0.502	0.465	0.496
	Mg	0.814	0.836	0.96	0.883	0.785	0.847	0.637	0.799
	Ca	0.892	0.891	0.923	0.876	0.847	0.844	0.836	0.847
	Total	3.912	3.94	3.982	3.966	3.892	3.971	3.853	3.947
Xmol(3)	Di	77.31	73.8	84.24	70.3	69.52	59.34	60.32	59.96
	En	2.02	4.89	5.89	9	4.5	12.7	1.69	9.97
	CaTs	3.04	9.31	6.22	13.94	4.35	22.2	8.51	19.52
	CaEs	17.62	12	3.65	6.76	21.63	5.77	29.48	10.56

No. exp.		A119	A120	A121	A122	A124	A125	A127	A128
Analyses[1] wt%	SiO_2	54.24	52.83	50.43	49.75	56.21	54.17	51.94	49.84
	Al_2O_3	4.35	7.05	12.31	16.36	11.08	5.98	8.26	12.28
	MgO	17.49	16.3	15.31	13.54	12.03	16.13	16.65	15.41
	CaO	23.7	23.31	21.93	20.48	21.06	23.37	22.79	22.1
	Total	99.77	99.49	99.97	100.14	100.38	99.66	99.64	99.62
a.p.f.u.[2]	Si	1.941	1.894	1.791	1.75	1.955	1.935	1.858	1.78
	Al	0.183	0.298	0.515	0.678	0.454	0.252	0.348	0.517
	Mg	0.933	0.871	0.81	0.71	0.624	0.859	0.888	0.82
	Ca	0.909	0.895	0.834	0.772	0.785	0.894	0.874	0.845
	Total	3.967	3.958	3.951	3.911	3.818	3.94	3.968	3.962
Xmol[3]	Di	81.71	74.61	57.69	43.29	55.77	76.85	69.94	58.71
	En	5.82	6.25	11.68	13.87	3.31	4.52	9.42	11.67
	CaTs	5.86	10.65	20.88	24.99	4.48	6.55	14.18	22.04
	CaEs	6.61	8.49	9.75	17.85	36.44	12.09	6.46	7.59
No. exp.		A129	A132	A133	A134	A135	A136	A140	P42
Analyses[1] wt%	SiO_2	49.4	55.48	54.72	49.94	49.98	52.7	54.96	54.59
	Al_2O_3	16.61	13.75	4.37	11.52	16.64	8.38	2.46	5.12
	MgO	13.16	11.56	16.71	17.43	13.23	16.94	18.57	16.1
	CaO	20.88	19.75	24.42	21.74	20.44	22.44	24.47	24.61
	Total	100.04	100.53	100.22	100.62	100.28	100.46	100.46	100.41
a.p.f.u.[2]	Si	1.742	1.917	1.951	1.768	1.754	1.865	1.961	1.943
	Al	0.69	0.56	0.184	0.48	0.688	0.35	0.103	0.215
	Mg	0.692	0.595	0.889	0.92	0.692	0.894	0.988	0.854
	Ca	0.789	0.731	0.933	0.824	0.768	0.851	0.936	0.938
	Total	3.913	3.803	3.957	3.992	3.902	3.96	3.987	3.95
Xmol[3]	Di	44.38	45.13	84.11	58.41	42.45	67.63	88.4	83.11
	En	12.39	7.21	2.37	16.78	13.37	10.86	5.19	1.14
	CaTs	25.8	8.32	4.85	23.23	24.63	13.47	3.92	5.73
	CaEs	17.43	39.35	8.66	1.57	19.56	8.04	2.5	10.02
No. exp.		P48	P56	P429	P438	P439	P441	P442	P444
Analyses[1] wt%	SiO_2	52.45	44.98	54.73	51.45	52.17	51.97	53.36	49.84
	Al_2O_3	10.16	28.53	4.98	9.33	6.72	9.67	6.98	11.66
	MgO	13.07	4.21	16.03	14.89	15.99	14.6	14.6	13.71
	CaO	24.57	22.18	24.46	23.88	25	23.51	24.79	24.54
	Total	100.25	99.92	100.2	99.54	99.87	99.75	99.73	99.75

a.p.f.u.[2]	Si	1.866	1.583	1.95	1.847	1.908	1.856	1.913	1.79
	Al	0.426	1.184	0.209	0.394	0.25	0.407	0.295	0.494
	Mg	0.693	0.221	0.852	0.797	0.854	0.777	0.78	0.734
	Ca	0.936	0.837	0.934	0.918	0.955	0.9	0.952	0.945
	Total	3.921	3.825	3.945	3.956	3.967	3.94	3.94	3.963
Xmol[3]	Di	68.3	21.83	82.94	72.09	82.07	69.62	77.07	69.77
	En(Wo)			1.11	3.79	1.82	4.06		1.82
	CaTs	13.24	41.17	4.96	15.33	12.39	14.38	8.62	20.96
	CaEs	15.51	34.65	10.99	8.78	3.73	11.94	11.88	7.44
No. exp.		P445	P447	P448	P450	P451	P454	P457	P458
Analyses[1] **wt%**	SiO_2	50.87	52.1	50.32	53	55.2	55.63	54.34	52.06
	Al_2O_3	6.73	9.23	4.6	7.08	4.09	1.57	2.57	8.4
	MgO	15.51	15.03	15.91	16.09	16.46	18.38	17.43	15.82
	CaO	25.52	23.58	23.41	23.94	24.53	25.29	25.07	23.63
	Total	98.63	99.94	94.24	100.1	100.28	100.86	99.41	99.91
a.p.f.u.[2]	Si	1.86	1.875	1.916	1.899	1.966	1.981	1.963	1.861
	Al	0.29	0.376	0.206	0.318	0.172	0.066	0.109	0.354
	Mg	0.845	0.791	0.903	0.822	0.874	0.975	0.939	0.843
	Ca	1	0.895	0.955	0.903	0.936	0.965	0.97	0.905
	Total	3.995	3.937	3.981	3.942	3.948	3.987	3.982	3.962
Xmol[3]	Di	85.5	70.73	85.19	76.65	85.03	93.18	91.58	72.8
	En		4.61	2.56	4.47	1.18	2.19	1.15	5.75
	CaTs	14	14.15	8.39	10.88	3.39	1.95	3.67	13.93
	CaEs	1	10.51	3.86	7.99	10.4	2.69	3.6	7.52
No. exp.		P459	P461	P462	P463	P464	P465	P466	P467
Analyses[1] **wt%**	SiO_2	48.99	46.32	52.98	53.2	52.53	54.05	53.2	52.16
	Al_2O_3	13.94	22.81	5.85	4.61	7.42	2.96	6.14	5.91
	MgO	11.89	7.96	16.22	16.64	16.1	17.84	16.64	17.37
	CaO	24.5	22.97	25.09	25.44	24.2	24.93	24.47	24.54
	Total	99.33	100.06	100.14	99.89	100.25	99.78	100.46	99.98
a.p.f.u.[2]	Si	1.764	1.64	1.899	1.877	1.875	1.946	1.901	1.875
	Al	0.592	0.952	0.247	0.279	0.312	0.126	0.252	0.25
	Mg	0.638	0.42	0.867	0.865	0.857	0.958	0.89	0.931
	Ca	0.945	0.871	0.964	0.962	0.925	0.962	0.929	0.945
	Total	3.94	3.884	3.977	3.983	3.969	3.991	3.973	4
Xmol[3]	Di	63.48	39.55	84.02	88.37	76.94	89.9	80.58	81.98

	En(Wo)		1.23	1.33	0.48	4.36	2.93	3.94	5.54
	CaTs	23.43	35.98	10.07	8.43	12.51	5.39	10.32	12.55
	CaEs	11.97	23.23	4.58	2.72	6.18	1.78	5.16	
No. exp.		P468	P470	P471	P472	P473	P475	P481	P498
Analyses(1) wt%	SiO_2	48.84	48.56	52.67	53.27	50.27	54.38	53.74	48.82
	Al_2O_3	9.96	15.67	5.96	4.63	12.57	3.13	6.14	15.15
	MgO	14.08	11.45	16.33	16.77	13.18	17.94	15.63	14.85
	CaO	25.84	23.89	25.05	25.23	23.63	24.66	24.72	21.25
	Total	98.72	99.57	100.01	99.9	99.65	100.11	100.23	100.07
a.p.f.u.(2)	Si	1.787	1.74	1.878	1.917	1.813	1.948	1.918	1.73
	Al	0.43	0.662	0.292	0.973	0.888	0.132	0.258	0.633
	Mg	0.768	0.611	0.854	0.9	0.679	0.958	0.831	0.785
	Ca	1.013	0.917	0.953	0.196	0.538	0.947	0.945	0.807
	Total	3.998	3.93	3.976	3.985	3.918	3.986	3.953	3.954
Xmol(3)	Di	75.7	58.62	83.78	87.45	64.09	88.08	81.63	49.05
	En(Wo)		1.26	1.82	1.25	3.1	3.87	0.75	14.7
	CaTs	21	26.04	10.84	8.33	20.18	5.17	8.19	27.02
	CaEs	0.4	14.07	3.56	2.97	12.63	2.88	9.42	9.23
No. exp.		P499	P509	P510	P521	P522	P523	P524	P525
Analyses(1) wt%	SiO_2	54.9	51.94	50.47	56.8	49.6	53	53.67	50.25
	Al_2O_3	2.57	7.33	16.63	2.53	16.49	8.98	4.67	16.97
	MgO	19.77	17.3	12.97	17.4	13.41	15.67	16.66	13.23
	CaO	22.77	22.64	20.72	24.89	19.69	22.28	24.56	20.19
	Total	100.01	99.21	100.79	101.62	99.19	99.92	99.55	100.64
a.p.f.u.(2)	Si	1.958	1.867	1.762	1.997	1.756	1.881	1.931	1.754
	Al	0.108	0.311	0.684	0.105	0.688	0.375	0.198	0.698
	Mg	1.051	0.927	0.675	0.912	0.708	0.829	0.894	0.689
	Ca	0.87	0.872	0.775	0.937	0.747	0.847	0.947	0.755
	Total	3.988	3.977	3.896	3.951	3.9	3.932	3.97	3.896
Xmol(3)	Di	81.62	71.68	43.29	88.51	40.31	65.93	84.79	40.61
	En	11.75	10.52	12.1	1.34	15.25	8.47	2.29	14.12
	CaTs	4.18	13.26	23.81	0.33	24.37	11.94	6.87	24.56
	CaEs	2.45	4.53	20.79	9.82	20.07	13.66	6.04	20.7
No. exp.		P526	P535	P536	P554	P555	P558	P561	P562
Analyses(1)	SiO_2	51.96	49.89	52.96	55.73	55.25	52.95	55.2	54.51

wt%	Al_2O_3	7.79	16.31	8.8	6.43	5.55	6.05	4.02	3.69
	MgO	17.16	15.45	16.14	15.07	16.18	16.4	17.37	17.96
	CaO	22.65	19.15	22.68	23.7	23.85	24.91	24.88	24.28
	Total	99.56	100.79	100.58	100.92	100.84	100.31	101.46	100.45
a.p.f.u.[(2)]	Si	1.861	1.739	1.871	1.959	1.95	1.894	1.948	1.943
	Al	0.329	0.67	0.366	0.266	0.231	0.255	0.167	0.155
	Mg	0.916	0.803	0.85	0.79	0.851	0.875	0.913	0.954
	Ca	0.869	0.715	0.858	0.892	0.902	0.955	0.941	0.927
	Total	3.975	3.926	3.946	3.908	3.934	3.978	3.969	3.98
Xmol[(3)]	Di	70.46	38.02	67.52	75.93	78.66	82.72	85.72	84.99
	En	10.57	21.12	8.75	1.51	3.24	2.37	2.81	5.23
	CaTs	13.91	26.12	12.9	4.08	4.99	10.59	5.23	5.72
	CaEs	5.05	14.74	10.83	18.47	13.11	4.32	6.23	4.07
No. exp.		P564	P565	P567	P568				
Analyses[(1)] **wt%**	SiO_2	54.06	55.26	53.33	53.01				
	Al_2O_3	3.9	2.4	4.23	7.86				
	MgO	17.88	18.45	16.17	15.2				
	CaO	24.03	24.31	24.91	23.24				
	Total	99.88	100.41	98.64	99.32				
a.p.f.u.[(2)]	Si	1.937	1.97	1.94	1.899				
	Al	0.165	0.101	0.181	0.332				
	Mg	0.955	0.98	0.877	0.812				
	Ca	0.923	0.929	0.971	0.892				
	Total	3.98	3.98	3.969	3.935				
Xmol[(3)]	Di	84.03	87.83	87.55	72.62				
	En(Wo)	5.76	5.1		4.27				
	CaTs	6.25	3	5.99	10.09				
	CaEs	3.96	4.06	6.13	13.03				

Note. [(1)] analyses obtained by Energy-dispersive spectrometry (EDS), wt.%; [(2)] atomic per formula unit on the basis of 6 oxygens; [(3)] end members, mol.%.

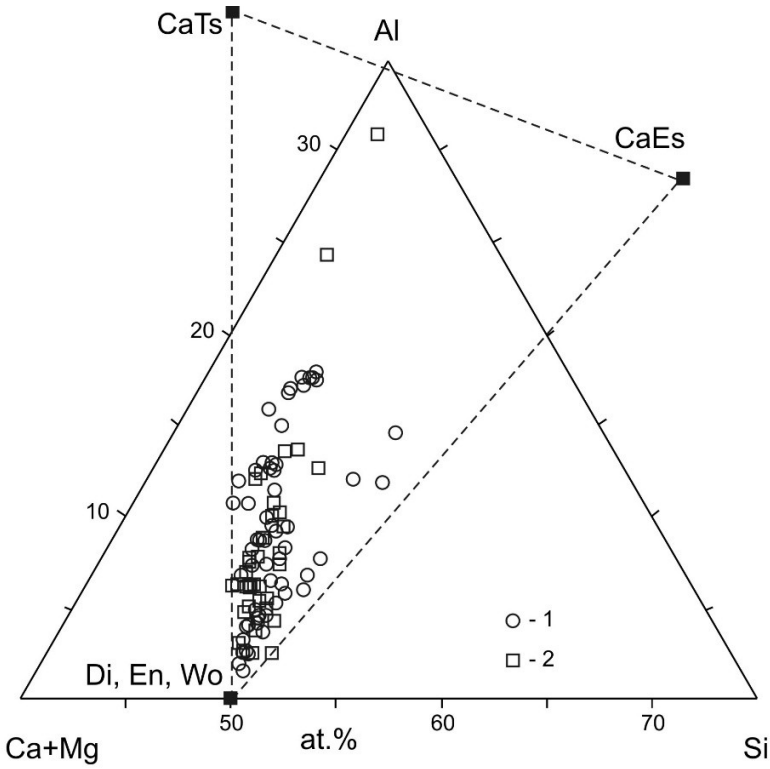

Figure 9. Clinopyroxene solid solution compositions. 1 - new data, 2 - data previously published (Surkov et al., 2004; Surkov et al., 2007; Surkov et al., 2018; Banushkina et al., 2019).

The content of Al^{3+} in Cpx(ss) is proportional to the bulk composition of the system. At 1 atm, the minimum Al_2O_3 value is 1.21 mol.% for $Di_{95}CaEs_5$ at 1238 ºC, and the maximum is ~8-9 mol.% for $Di_{30}CaEs_{70}$ at 1013 ºC. For high-pressure conditions, such approximation is not sufficiently pronounced. The minimum Al_2O_3 value is 1.34 mol.% (1.2 GPa; 1208 ºC; $Di_{80}CaEs_{20}$). There are slight variations of Al_2O_3 in Cpx with increasing temperature and the amount of CaEs end-member in the starting material (x_i). Values do not exceed 4-5 mol.%.

Additionally, the amount of Al_2O_3 in Cpx(ss) decreases in the presence of Grt (and An), which is consistent with (Kushiro, 1969; Knapp et al., 2013). This is due to the better accommodation in a garnet lattice compared to a clinopyroxene one. For example, for $Di_{50}CaEs_{50}$ at 1218±10 ºC, the Al_2O_3 content is 9.19 mol.% in experiment P-470, but in experiment P-444 in the presence of Grt, this value is 6.64 mol.%.

The dependence of the molar fraction of CaTs and CaEs components on the amount of Al in the bulk composition is shown in Fig. 10. There is a positive correlation between these values, which is more distinct for the CaTs end member (Banushkina et al., 2020), corresponding to similar results previously published by Knapp et al. (Knapp et al., 2013).

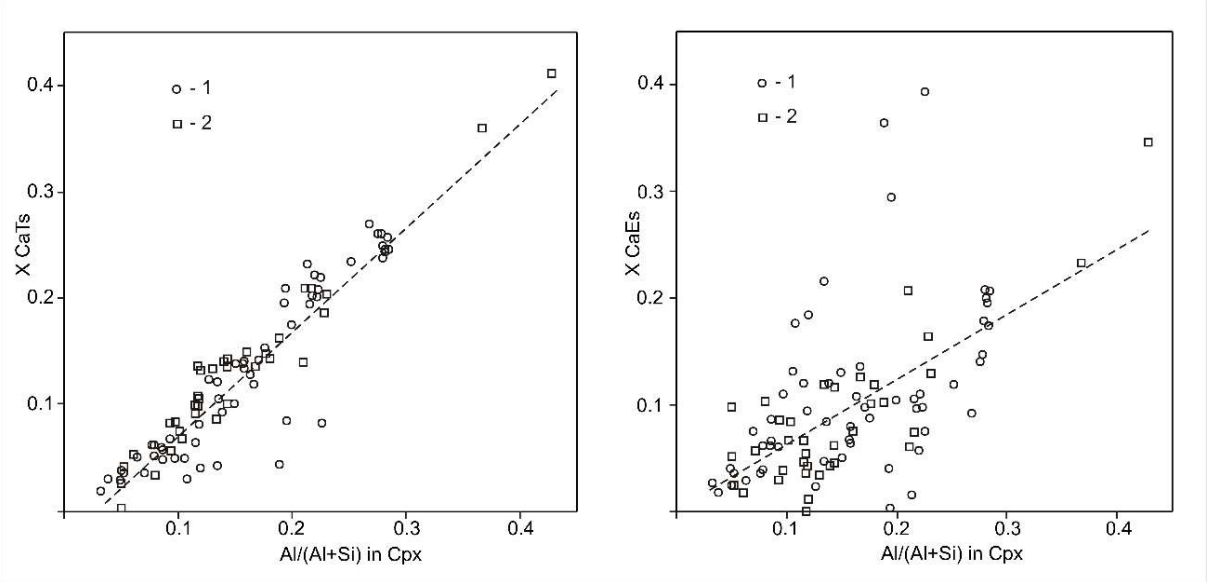

Figure 10. Calculated CaTs and CaEs contents plotted as a function of molar Al/(Al+Si) in clinopyroxene. 1 - new data, 2 - data previously published (Surkov et al., 2004; Surkov et al., 2007; Surkov et al., 2018; Banushkina et al., 2019).

It should also be noted that garnet belongs to the solid solutions of the pyrope (Prp) - grossular (Grs) series, with the amount of Prp component being ~3-6 mol.%. An, Qtz, and Tr correspond to stoichiometry; the composition of melt L is mainly calcium and siliceous.

4. Discussion

We have reviewed the Di-CaEs section of the 'dry' CMAS system at pressures from 1 atm to 3.0 GPa and in the temperature range of 960-1550±10 ºC. We assumed that Di and CaEs end members would describe the composition of clinopyroxene obtained. However, there are two independent stable pyroxene phases in the association. The composition of Al-bearing Cpx is represented by the quad series of end members Di-En-CaTs-CaEs. The high-magnesium Di found in the run products does not belong to this series because it is characterized by the absence of Al_2O_3 in its structure. We assume a narrow field of miscibility breaks. At the same time, an excess of En component from 1 to 5 mol.% was noted in the Di composition. Hence, this field of miscibility break should be slightly shifted in the direction of En. The Di-En-CaTs-CaEs tetrahedron occupies a central position in the CMAS system (Fig. 11).

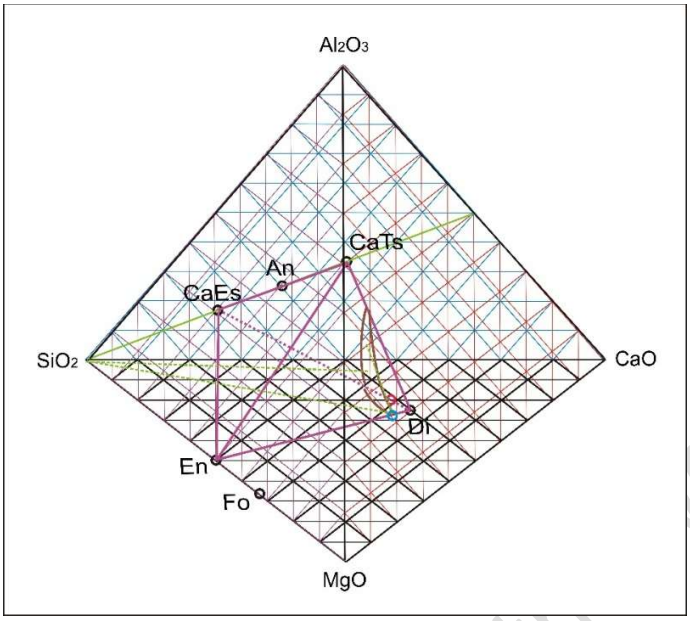

Figure 11. CMAS system. The starting composition (red spot) is schematically located on the Di-CaEs cross-section (purple dotted line). Al-bearing Cpx(ss) are inside the Di-En-CaTs-CaEs tetrahedron (purple). The Di composition (blue spot) is schematically marked on the Di-En line.

It was shown that the content of Al_2O_3 in Cpx(ss) is proportional to the bulk composition of the system and depends on the association of coexisting phases. In the *P-T* range studied, CaEs content in the run products is mainly 3-15 mol.%. High values are typical for bulk compositions with CaEs >50 mol.% in the starting material (Fig. 12). At the same time, the presence of An or Grt reduces the content of CaEs in the run products. Thus, bulk chemical composition is the most important variable, while temperature and pressure have little effect on CaEs content in Cpx. This conclusion is fully consistent with results known (Konzett et al., 2008; Zhao et al., 2011; Knapp et al., 2013).

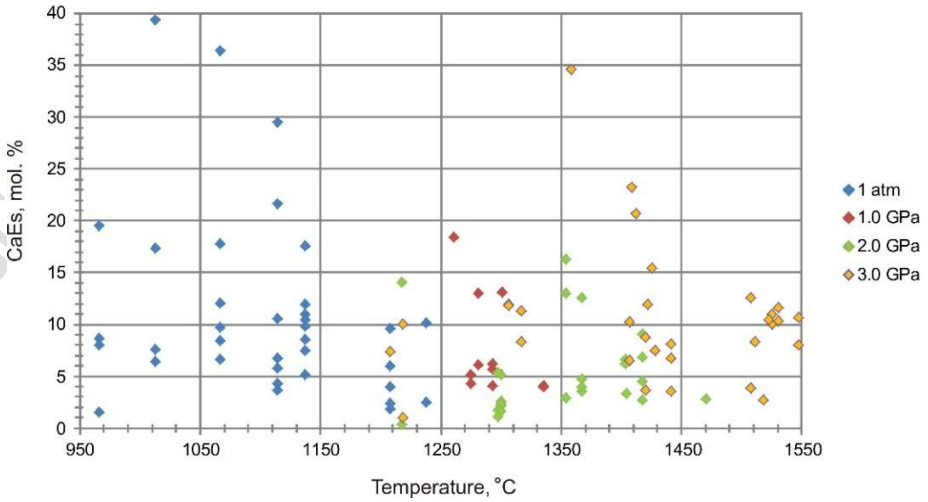

Figure 12. Content of CaEs end member in Cpx.

We do not observe thin oriented needles of an SiO_2 polymorph as seen in the works (Janak et al., 2004; Konzett et al., 2008; Zhao et al., 2011; Schroeder-Frerkes et al., 2016). Such needles could indicate the decay process CaEs = CaTs + $3SiO_2$ (Su et al., 2001; Katayama and Maruyama, 2009). The reason lies in the starting materials used. Natural samples in works (Janak et al., 2004; Katayama and Maruyama, 2009) contain many minor components (Fe, Na, etc.). The synthetic CMAS system in works (Konzett et al., 2008; Zhao et al., 2011; Schroeder-Frerkes et al., 2016) also includes Na, oxides of Fe and Ti, and volatile components. A complex composition better approximates the natural features observed. However, a simple system like CMAS makes it possible to model geological processes.

Two pyroxenes can explain the low temperatures at which the melt appears. According to thermodynamics laws, the addition of Di in associations (Cpx + An + Qtz) and (Cpx + Grt + Qtz) leads to the formation of new monovariant eutectic equilibria. As a result, the melting temperature of the system decreases. In the quartz-normative area of CMAS studied, we observed the melting of compositions from 1137±10 ºC (at 1 atm) to 1300±10 ºC and higher (at 3.0 GPa). This eutectic trend is about 150-200 °C lower than for forsterite- and corundum-normative areas. Understanding how the CaEs end member behaves as a function of *P*, *T*, and composition is of petrologic importance. CaEs participates in the formation of quartz (coesite) eclogites (Knapp et al., 2015). During tectonic uplift of bodies, coesite can be exsolved from clinopyroxene. V.S. Sobolev shares this opinion, considering coesite eclogites as one of the sources of mantle magmas of acidic and intermediate composition (Sobolev, 1979). Xenoliths of coesite eclogites (e.g., Yakutia) and grospidites (Roberts-Victor, South Africa) have been found in kimberlite pipes. They can form due to the sinking of tholeiitic basalts in the Zavaritsky-Benioff zones or eclogitization of the lower part of the continental crust with the separation of corresponding blocks. Another option may be the process of crystallization differentiation. New data obtained and previous results allow for building a phase diagram with trends of eutectic crystallization. Such a model is logically closest to Bowen's theory of crystallization differentiation. It offers one of the possible ways of magmatic melt evolution and allows overcoming the so-called 'eclogite barrier' (Sobolev, 1979; Zharikov, 1984). This is the subject of a separate article.

Acknowledgments

The authors are sincerely grateful to Silvio RF Vlach and two anonymous reviewers for their valuable comments. This work was carried out according to the state assignment of the V.S. Sobolev Institute of Geology and Mineralogy of the Siberian Branch of the Russian Academy of Sciences (project No.122041400057-2).

References

Banushkina S.V., Kirdyashkin A.A., Golitsyna Z.F. (2025) High-pressure experiments in petrological researches by piston-cylinder device method. *Iranian Journal of Earth Sciences* (in press).

Banushkina S.V., Surkov N.V., Golitsyna Z.F. (2019) Melting features of phases in the diopside Calcium molecule of Escola section in the pressure range 1 kg/sm^2 – 20 kbar. *Transbaikal State University Journal* 25 (7):6–17. DOI: https://doi.org/10.21209/2227-9245-2019-25-7-6-17 (in Russian)

Banushkina S.V., Turkin A.I., Chepurov A.I. (2020) Clinopyroxene Solid Solutions in the $CaMgSi_2O_6$–$Ca_{0,5}AlSi_2O_6$ Cross-Section at High PT Parameters. *The bulletin of Irkutsk State University. «Series Earth Sciences»* 34: 37-54. DOI: https://doi.org/10.26516/2073-3402.2020.34.37

Bruno M., Compagnoni R., Hirajima T., Rubbo M. (2002) Jadeite with the Ca-Eskola molecule from an ultra-high pressure metagranodiorite, Dora-Maira Massif, Western Alps. *Contributions to Mineralogy and Petrology* 142:515-519. DOI: https://doi.org/10.1007/s004100100307

Day H.W., Mulcahy S.R. (2007) Excess silica in ophacite and the formation of free silica in eclogite. *Journal of metamorphic Geology* 25:37-50. DOI: https://doi.org/10.1111/j.1525-1314.2006.00677.x

Eskola P. (1921) On the eclogites of Norway. Videnskaps-selskapets Skr. J., Kristiania. I. Matematisk-Naturvidenskapelig. kl., Oslo 8:163-170.

Gasparik T. (2013) System CaO-MgO-Al_2O_3-SiO_2 Saturated with Silica. In: Phase Diagrams for Geoscientists. *Springer,* New York, NY:173-213. DOI: https://doi.org/10.1007/978-1-4614-5776-3_6

Gonzaga R.C., Lowry D., Jacob D.E., LeRoex A., Schulze D., Menzies M.A. (2010) Eclogites and garnet pyroxenites: Similarities and differences. *Journal of Volcanology and Geothermal Research*. *Special Issue*: Making and Breaking the Arc: A Volume in Honour of Professor John Gamble; ed. J. Marti 190:235-247. DOI: https://doi.org/10.1016/j.jvolgeores.2009.08.022

Ishbulatov R.A. (1977) Experimental studies of the melting of alkali earth rock series at pressures of 25-45 kbar. Contributions to Physicochemical Petrology. *MOSCOW: Science* 6:97-167 (in Russian).

Ishbulatov R.A., Chudinovskikh L.T., Malinovskaya E.K. (1986) Experimental researches of solubility of end member $Ca_{0,5}AlSi_2O_6$ in clinopyroxenes at pressures from 14 up to 70 kbar. *Proceedings of XIII Congress of International Mineralogical Association (IMA);* 1982 19-25 sept; Varna, Bulgaria: Ser. Bulg. AS Crystallochem. Min. 1986:351-357 (in Russian).

Janak M., Froitzheim N., Luptak B., Vrabec M., Ravna E. (2004) First evidence for ultrahigh-pressure metamorphism of eclogites in Pohorje, Slovenia: Tracing deep continental subduction in the Eastern Alps. *Tectonics* 23 (TC5014):1–10. DOI: https://doi.org/10.1029/2004TC001641

Katayama I., Maruyama S. (2009) Inclusion study in zircon from ultrahigh-pressure metamorphic rocks in the Kokchetav massif: an excellent tracer of metamorphic history. *Journal of the Geological Society* 166:783–796. DOI: https://doi.org/10.1144/0016-76492008-019

Knapp N., Woodland A.B., Klimm K. (2013) Experimental constraints in the CMAS system on the Ca-Eskola content of eclogitic clinopyroxene. *European Journal of Mineralogy* 25 (4):579–596. DOI: https://doi.org/10.1127/0935-1221/2013/0025-2326

Knapp N., Woodland A.B., Klimm K. (2015) Experimental constraints on coesite abundances in eclogite and implications for the X seismic discontinuity. *Journal of Geophysical Researches: Solid Earth* 120:4917-4930. DOI: https://doi.org/10.1002/2015JB011933

Konzett J., Frost D.J., Proyer A., Ulmer P. (2008) The Ca-Eskola component in eclogitic clinopyroxene as a function of pressure, temperature and bulk composition: an experimental study to 15 GPa with possible implications for the formation of oriented SiO_2-inclusions in omphacite. *Contributions to Mineralogy and Petrology* 155:215-228. DOI: https://doi.org/10.1007/s00410-007-0238-0

Kushiro I. (1969) Clinopyroxene solid solutions formed by reactions between diopside and plagioclase at high pressures. *Mineralogy Society of America*. *Special* 2:179-191.

Lavrent'ev Y.G., Karmanov N.S., Usova L.V. (2015) Electron probe microanalysis of minerals: microanalyzer or scanning electron microscope? *Russian Geology and Geophysics* 56 (8):1154–1161. DOI: https://doi.org/10.1016/j.rgg.2015.07.006

Ousta S.h., Ashja-Ardalan A., Yazdi A., Dabiri R., Arian M.A. (2024) Petrogenesis and tectonic implications of Miocene dikes in the southeast of Bam (SE Iran): Constraints on the development of active continental margin, *Geopersia* 14 (1): 89-111. DOI: https://doi.org/10.22059/geope.2023.364334.648729

Ravna E.J.K., Paquin J. (2003) Thermobarometric methodologies applicable to eclogites and garnet ultrabasites. *In EMU Notes in Mineralogy, 5 (Chapter 8)*:229–259. DOI: https://doi.org/10.1180/EMU-notes.5.8

Revenaugh J., Jordan T.H. (1991) Mantle layering from ScS reverberations: 3. The upper mantle. *Journal of Geophysics Research* 96:19781-19810. DOI: https://doi.org/10.1029/91JB01487

Schroeder-Frerkes F., Woodland A.B., Uenver-Thiele L., Klimm K., Knapp N. (2016) Ca-Eskola incorporation in clinopyroxene: limitations and petrological implications for eclogites and related rocks. *Contributions to Mineralogy and Petrology* 171:100–118. DOI: https://doi.org/10.1007/s00410-016-1311-3

Sobolev N.V., Kuznetsova I.K., Zyuzin N.I. (1968) The petrology of grospydite xenoliths from the Zagadochnaya kimberlite pipe in Yakutia. *Journal of Petrology* 9 (2):253-280. DOI: https://doi.org/10.1093/petrology/9.2.253

Sobolev V.S. (1979) Coesite (quartz) eclogites as a source of mantle magmas rich in silica. Problems of deep magmatism: collection of scientific papers; ed. by V.S. Sobolev. *Moscow, Science*:7-11 (in Russian).

Su W., You Z., Wang R., Liu X. (2001) Quartz and clinoenstatite exsolutions in clinopyroxene of garnet-pyroxenolite from the North Dabie Mountains, eastern China. *Chinese Science Bulletin* 46 (17):1482–1484. DOI: https://doi.org/10.1007/BF03187037

Surkov N.V., Banushkina S.V., Gartvich Yu.G. (2018) Melting of associations with a-diopside in the $CaMgSi_2O_6$-$Ca_{0,5}AlSi_2O_6$ section at atmospheric pressure. *Transbaikal State University Journal* 24 (7):51-59 (in Russian). DOI: https://doi.org/10.21209/2227-9245-2018-24-7-51-59

Surkov N.V., Darmenko O.L. (2002) Experimental investigation of clinopyroxene stability in the section Di-CaTs-CaEs at pressure 30 kbar. *Experiment in Geoscience* 10 (1):32-34.

Surkov, N.V., Gartvich Y.G., Babich Y.V. (2004) Experimental study of the phase diagram of CaMgSi2O6 - CaAl0,5Si2O6 system at 3.0 GPa. *Doklady earth sciences. Pleiades Publishing, Ltd* 398 (7):1038-1042.

Surkov N.V., Gartvich Y.G., Izokh O.P. (2007) Stability and phase relations of nonstoichiometric clinopyroxenes in the join diopside - Ca-Eskola component at high pressures. *Geochemistry International* 45 (6):569-579. DOI: https://doi.org/10.1134/S0016702907060055

Talebian Borojenie H, Sheykhzakariaei S.J., Dabiri R., Yazdi A. (2025) Petrogenesis and tectonic implications of Neoproterozoic to Cenozoic A-type granitoids in NW Iran: geochemical and tectonic constraints, Iranian Journal of Earth Sciences, 17(4): 1-19. DOI: https://doi.org/10.57647/j.ijes.2025.16894

Williams Q., Revenaugh J. (2005) Ancient subduction, mantle eclogite, and the 300km seismic discontinuity. *Geology* 33:1-4. https://doi.org/10.1130/G20968.1.

Yoder H.S.Jr., Tilley C.E. (1962) Origin of Basalt Magmas: An Experimental Study of Natural and Synthetic Rock Systems. *Journal of Petrology* 3 (part 3):342-532. DOI: https://doi.org/10.1093/petrology/3.3.342

Zhao S., Nee P., Green H.W., Dobrzhinetskaya L.F. (2011) Ca-Eskola component in clinopyroxene: Experimental studies at high pressures and high temperatures in multianvil apparatus. *Earth and Planetary Science Letters* 307 (3-4):517–524. DOI: https://doi.org/10.1016/j.epsl.2011.05.026

Zharikov V.A., Ishbulatov R.A., Chudinovskikh L.T. (1984) High-pressure clinopyroxenes and the eclogite barrier. *Soviet Geology and Geophysics* 25:54-63.